Received: 4 November 2017 | Revised: 10 January 2018 | Accepted: 23 January 2018

DOI: 10.1002/cne.24435

RESEARCH ARTICLE

WILEY JCN RESEARCH IN SYSTEMS NEUROSCIENCE THE JOURNAL OF COMPARATIVE NEUROLOGY

Distribution of cytochrome oxidase-rich patches in human primary visual cortex

Marco Marcondes[1,2] | Marcello G.P. Rosa[1,3,4] | Mario Fiorani[1] | Bruss Lima[1] | Ricardo Gattass[1]

[1]Programa de Neurobiologia, Instituto de Biofísica Carlos Chagas Filho, Universidade Federal do Rio de Janeiro, Rio de Janeiro, RJ 21941, Brazil

[2]Departamento de Ciências Fisiológicas, Universidade de Brasília, Brasília, DF, Brazil

[3]Department of Physiology and Biomedicine Discovery Institute, Monash University, Clayton, VIC 3800, Australia

[4]Australian Research Council, Centre of Excellence for Integrative Brain Function, Monash University Node, Clayton, VIC 3800, Australia

Correspondence
Ricardo Gattass, Instituto de Biofísica Carlos Chagas Filho, Bloco G, CCS, Universidade Federal do Rio de Janeiro, Cidade Universitária, Ilha do Fundão, Rio de Janeiro, RJ, 21941-902, Brazil.
Email: rgattass@gmail.com

Funding information
Fundação Carlos Chagas Filho de Amparo à Pesquisa do Estado do Rio de Janeiro, Grant/Award Number: E-26/110.192/2013, E-26/110.905/2013; Financiadora de Estudos e Projetos, Grant/Award Number: PEC20150; Conselho Nacional de Desenvolvimento Científico e Tecnológico, Grant/Award Number: 471.166/2013-8; Australian Research Council, Grant/Award Number: CE140100007; Serrapilheira Institute (grant# Serra-1709-17523)

Abstract

We studied the tangential distribution of cytochrome oxidase (CytOx)-rich patches (blobs) in the striate cortex (V1) of normally sighted *Homo sapiens*. We analyzed the spatial density and cross-sectional area of patches in CytOx-reacted tangential sections of flat-mounted preparations of V1 and surrounding areas. CytOx-rich patches were most clearly defined in the supragranular cortical layers of V1, particularly at middle levels of layer III. Variations in patch spatial density were subtle across different visual eccentricity representations. Within the binocular representation of V1, the average patch spatial density decreased slightly with increasing cortical eccentricity, from around 1.0 patch/mm^2 in the foveal representation to 0.6 patch/mm^2 at the representation of ~60° eccentricity, but seemed to increase again at the representation of the monocular crescent. Across the entire sample, the cross-sectional area of patches (i.e., patch size) varied from approximately 0.2–0.8 mm^2, with a mean value of 0.32 mm^2. Notably, there was no significant variation in the mean patch size across eccentricity representations. Human patches are on average larger than those reported for nonhuman primate brains, and analysis of species with different brain sizes suggests an approximately linear relationship between V1 area and patch size. The relative constancy of patch metrics across eccentricities is in stark contrast with the exponential variation in V1 cortical magnification, suggesting a nearly invariant modular organization throughout human V1.

KEYWORDS
blob, cytochrome oxidase, modular organization, patches, striate cortex, V1

1 | INTRODUCTION

The concept of modular processing is central to models about how visual information is analyzed in the primary visual area (V1). Although a repetitive columnar arrangement of functionally similar elements has long been considered a fundamental principle of neocortical organization (Lorente de Nó, 1949; Mountcastle, 1978), initial formulations of the modular concept as applied to V1 were derived from the electrophysiological and anatomical studies of Hubel and Wiesel (1977). According to these, and subsequent studies using other methods (e.g., Blasdel & Salama, 1986; Löwel & Singer, 1987; Ts'o, Frostig, Lieke, & Grinvald, 1990), individual V1 modules, each approximately 2 mm^2, were theorized to contain all neural machinery needed for the distributed processing of the different attributes of an image within a small portion of the visual field.

J_ID: Customer A_ID: CNE24435 Cadmus Art: CNE24435 Ed. Ref. No.: CASA-JCN-17-0256.R1 Date: 4-April-18 Stage: Page: 2

TABLE 1 Description of the six human cases (BH1–6) used in this study

Case	Age (years)	Death-autopsy interval (hr)	Glutaraldehyde fixation solution (%)	Fixation duration (hr)	Integrity of area V1
BH1	55	6	2.5	24	Complete
BH2	30	12	2.5	24	Incomplete
BH3	64	8	2.5	24	Complete
BH4	60	10	2.5	24	Incomplete
BH5	21	21	2.0	4	Complete
BH6	30	20	2.0	4	Incomplete

The fundamental modular nature of V1 organization was made more explicit by the discovery of a periodic arrangement in the distribution of the enzyme cytochrome *c* oxidase (CytOx), which is clearest in the upper layers of V1 (Horton & Hubel 1981). CytOx is a metabolic enzyme of the respiratory cycle located in mitochondria, which has been used as a marker for cortical modular organization in various cortical areas and species (Horton & Hubel, 1981; Horton 1984; Tootell, Silverman, De Valois, & Jacobs, 1983; Livingstone & Hubel, 1984; Carroll & Wong-Riley, 1984; Cusick, Gould, & Kaas, 1984; Wong-Riley & Carroll, 1984; Rosa, Gattass, & Soares, 1991; Rosa, Gattass, Fiorani, & Soares, 1992; Solodkin & Van Hoesen, 1996; Solomon, 2002). The darkly staining patches revealed by staining sections cut tangent to the surface of V1 for CytOx (also referred to as blobs [Livingstone & Hubel, 1984], spots [Tootell et al., 1983], puffs [Carroll & Wong-Riley, 1984] or dots [Tigges, Hendrickson, & Tigges, 1984; Hendrickson, 1985]) keep regular relationships with other types of modules (e.g., orientation, ocular dominance and color selective columns; Livingstone & Hubel, 1984; Bartfeld & Grinvald, 1992; Valverde Salzmann, Bartels, Logothetis, & Schüz, 2012), thus offering an opportunity to directly visualize how such modules vary across the surface of this area. Although these patches are most clearly defined in layer III, corresponding CytOx-rich and CytOx-poor sub-regions are also observed in the supra- and infragranular layers of V1, and only layer IVc stains homogeneously in this area (Rosa et al., 1991).

To date, the distributions of CytOx patches across the entire extent of V1 have been reported for various species of primates. Although the presence of CytOx patches has been well characterized in human brains (Horton & Hedley-Whyte, 1984; Wong-Riley et al., 1993; Tootell & Taylor, 1995; Adams, Sincich, & Horton, 2007), the extent to which their distribution varies across the extent of V1 has not been systematically analyzed. Here, we take advantage of techniques for flat mounting the cerebral cortex, which have enabled the reconstruction of modular patterns over wider expanses of brain tissue in other species (Horton, 1984; Olavarria & Van Sluyters, 1985; Tootell & Silverman, 1985; Löwel & Singer, 1987; Rosa, Gattass, & Fiorani, 1988; Rosa et al., 1991, 1992; Florence & Kaas, 1992; Tootell & Taylor, 1995; Tootell, Hamilton & Silverman, 1995; Sincich, Adams, & Horton, 2003), to describe the tangential distribution of V1 CytOx-rich patches in the brain of individuals with no history of retinal lesions (which can change the distribution of patches; Trusk, Kaboord, & Wong-Riley, 1990; Rosa et al., 1992; Horton & Hocking, 1996; Adams et al., 2007).

2 | METHOD

We studied six cerebral hemispheres from individuals with ages varying from 21 to 64 year old (Table 1). The brains were provided by the Death Certification Office in the City of São Paulo, Brazil (SVO/USP), following family consent. The interval between death and brain removal ranged from 6 to 21 hr, with shorter intervals allowing for better results following CytOx histochemical processing. The procedures and protocols followed the NIH Guidelines for the Use of Human Tissue and were approved by the IBCCF/UFRJ Research Ethics Committee. T1

The brains were removed from the skull through a bone flap craniotomy, and perfused through the carotid and vertebral arteries with 0.9% saline solution. Subsequently, the blood vessels and pia mater were carefully peeled off the cortical surface, in order to enable the opening of sulci, and to facilitate penetration of the fixation solution (Figure 1). We flat-mounted the posterior portion of the brain following a procedure modified from Tootell and Silverman (1985, Method II), which involves gradually dissecting the white matter and opening up the sulci (Figure 2). F1 F2

The tissue was then held between two parafilm-covered glass panels and immersed into a chilled solution of 2–2.5% glutaraldehyde/10% sucrose/0.1 M phosphate buffer solution for 6–24 hr. Due to limitations imposed by the size of the available microtome, the blocks were separated into smaller pieces after fixation (Figure 3), quickly frozen, and cut in 60-μm thick histological sections tangential to the pial surface. The sections were immediately mounted in gelatinized slides, dried at room temperature, and stored overnight in phosphate buffer at 4°C. CytOx histochemistry followed the protocol described by Silverman and Tootell (1987). The stained sections were dehydrated, defatted, coverslipped, and photographed under blue light illumination using a high contrast film (Kodalith, Kodak Co.). No single histological section encompassed the entire extent of the patch-containing cortical layers. Therefore, we reconstructed the complete pattern of CytOx layer III patches using photograph segments originating from different histological sections, using blood vessels as landmarks (Rosa et al., 1988). F3

Our main objectives were to quantify patch density and patch size across the entire extent of V1. We considered the extent of area V1 to be coincident with the region containing CytOx-rich patches in the supragranular layers, and a dark, homogeneously staining layer IV. In order to assign data to representations of specific parts of the visual

J_ID: Customer A_ID: CNE24435 Cadmus Art: CNE24435 Ed. Ref. No.: CASA-JCN-17-0256.R1 Date: 4-April-18 Stage: Page: 3

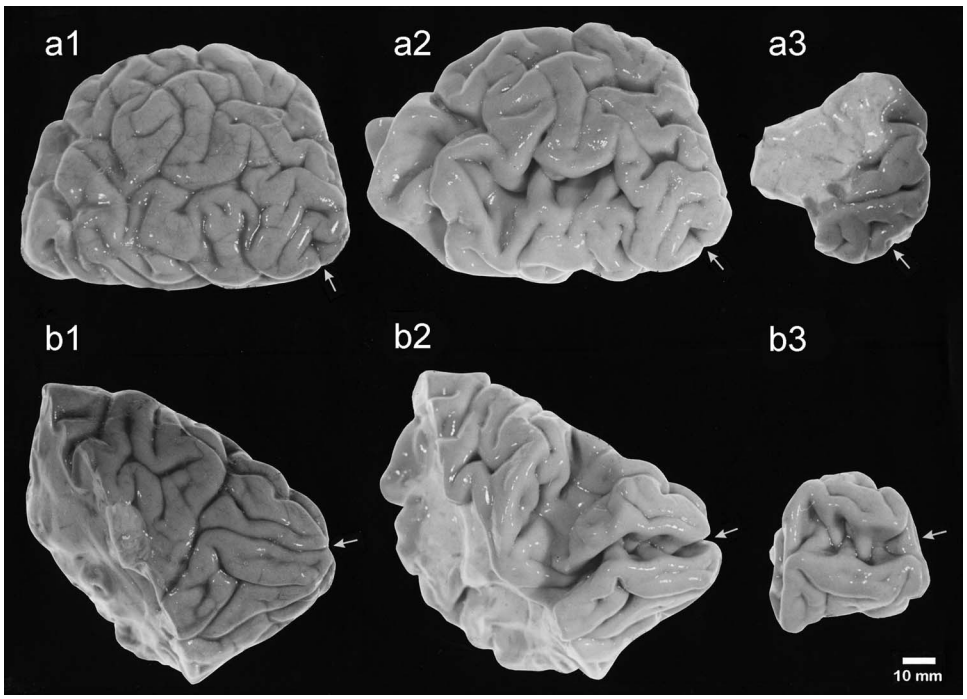

FIGURE 1 Pia removal and sulci opening prior to V1 flattening procedure. Sequence of steps (1–3) showing the removal of the pia and partial opening of the calcarine fissure viewed for both lateral (a) and medial (b) views of a human brain hemisphere. The occipital pole is located to the right of each panel. Arrows indicate the calcarine fissure. Note that we eventually isolate the occipital pole, which contains V1 and surrounding areas, from the rest of the brain before we initiate the flattening procedure (see Figure 2)

field we estimated the locations of isoeccentricity and isopolar contours to the flat-mounted V1 preparation, using modern descriptions of the human visuotopic map of V1 (Horton & Hoyt, 1991; Schira, Wade, & Tyler, 2007) as guides. To assign the location of isoeccentricity lines we used the numeric integration of a linear version of the magnification factor provided by Horton and Hoyt (1991), expressed by:

$$Mp = 17.3\ (ecc + 0.75)^{-1} \quad (1)$$

where *Mp* depicts the isopolar magnification factor, and *ecc* depicts the visual eccentricity representation. Since this procedure was applied across our six cases, which contained varying V1 sizes, we subsequently scaled individual estimates of the magnification factor by using the extent of the horizontal meridian (approximated as a line following the long axis of V1, and equidistant from its dorsal and ventral boundaries). The upper and lower halves of V1 were attributed, respectively, to the lower and upper quadrant representations of the contralateral visual hemifield (Gattass, Sousa, & Rosa, 1987; Sereno et al., 1995; Schira, Tyler, & Rosa, 2012; Chaplin, Yu, & Rosa, 2013). One example of such a map is shown in Figure 3 (bottom left insert; case BH5). To carry out our analysis, we subdivided V1 into 16 isoeccentric slices. Each slice was oriented roughly orthogonal to the representation of the horizontal meridian, and therefore contained visual representations within a certain isoeccentricity bin, distributed across all polar angles.

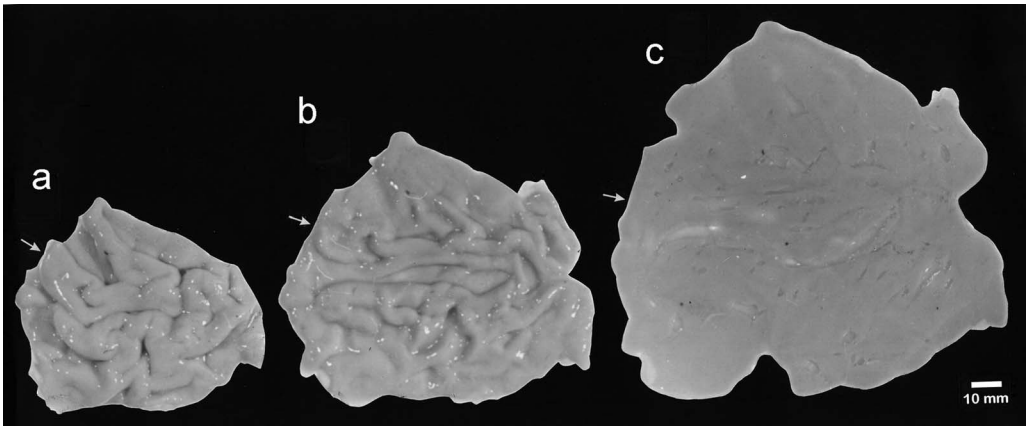

FIGURE 2 Steps undertaken to flatten area V1. Sequence of events (a–c) illustrating the dissection of the white matter from the occipital pole and the flattening of area V1 and surrounding areas. Arrows indicate the calcarine fissure

J_ID: Customer A_ID: CNE24435 Cadmus Art: CNE24435 Ed. Ref. No.: CASA-JCN-17-0256.R1 Date: 4-April-18 Stage: Page: 4

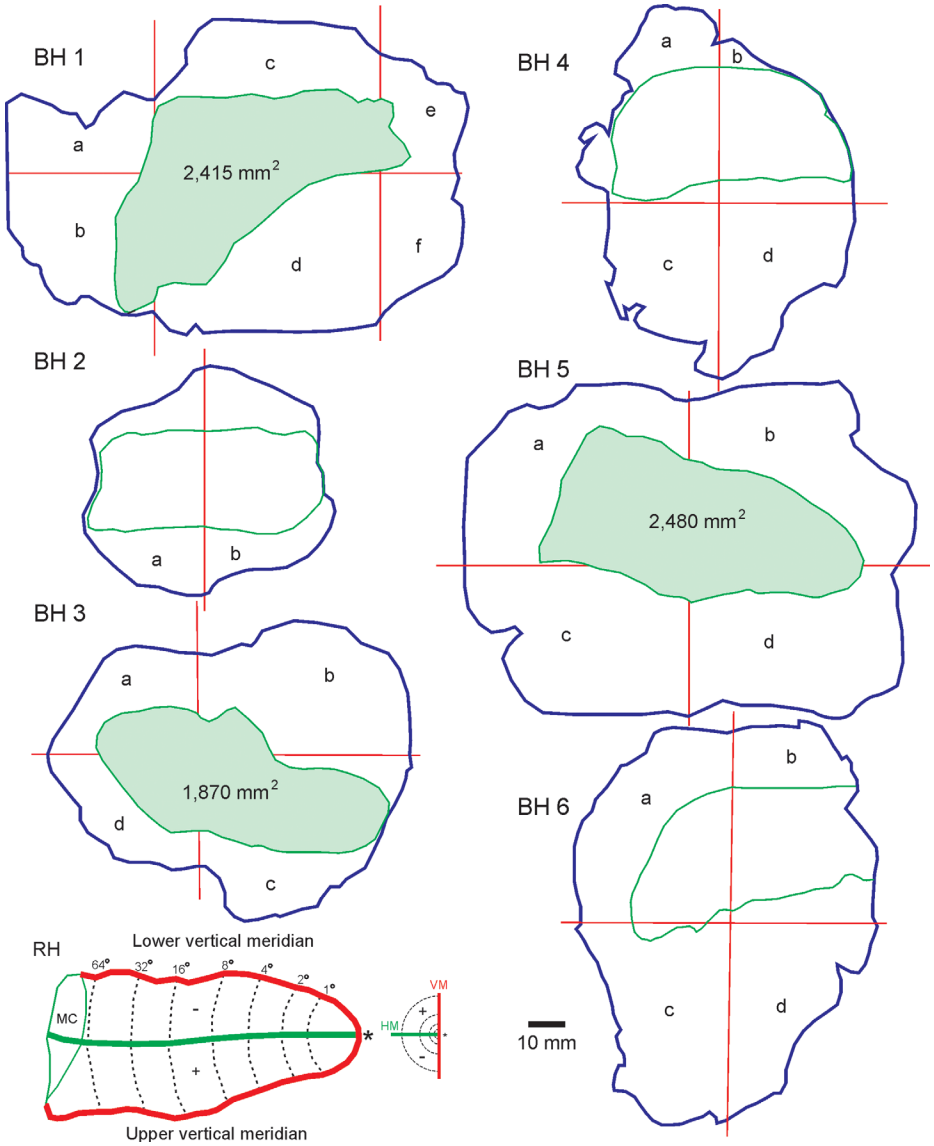

FIGURE 3 Illustrations of flattened area V1 for the six cases studied (BH1–6). Green outlines correspond to the limits of area V1. In three cases (BH1, 3 and 5) we were able to preserve the entirety of area V1 during the tissue processing procedure (see Figures 1 and 2). Preserved V1s are shown in filled green, and their estimated surface area is also depicted. Red lines indicate where the blocks were cut in order to obtain smaller tissue segments that fit into our freezing microtome. The bottom left insert illustrates the topographical organization of human area V1 for case BH5, alongside the corresponding representation of the left hemifield. HM, horizontal meridian; VM, vertical meridian; MC, monocular crescent. Scale bar = 10 mm [Color figure can be viewed at wileyonlinelibrary.com]

We quantified the distribution of patches based on a manual procedure whereby they were outlined on enlarged (5×), contrast-matched images of the flattened V1 reconstructions, using a fine-point permanent marker. Here, it is important to keep in mind that any estimates of patch boundaries are intrinsically dependent on determining a threshold between darkly and lightly staining tissue, a procedure which depends on factors such as the quality of the histological preparations, the photographic procedure, and, last but not least, human judgment. Although these factors are likely to affect estimates of patch size to a measurable extent (Purves & LaMantia, 1993), our experience was that human observers were remarkably consistent when asked to estimate patch boundaries on photographic print. We found no statistically significant difference in manual measurements of patch size and patch density performed by two independent experimenters on prints of the same photographs. Thus considered any individual bias that may have been introduced during the analysis to be negligible relative to the magnitude of the gradients across V1 that we report on.

3 | RESULTS

As previously described by Horton (1984), patches in human V1 are more conspicuous in the supragranular layers, particularly at the middle levels of layer III (Figure 4). The characteristic laminar profile of patch F4

J_ID: Customer A_ID: CNE24435 Cadmus Art: CNE24435 Ed. Ref. No.: CASA-JCN-17-0256.R1 Date: 4-April-18 Stage: Page: 5

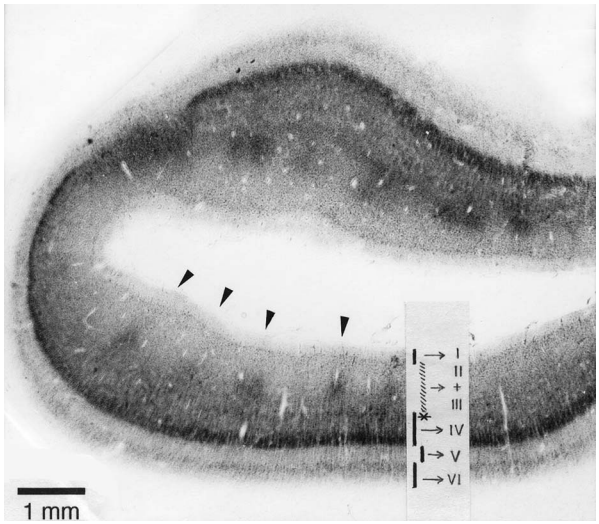

FIGURE 4 Patch profile across V1 cortical layers as evidenced by CytOx reactivity. Photomicrograph of a coronal section through the calcarine fissure stained for CytOx. Patches (depicted by arrow heads) are most evident in layer III of V1, especially in the middle of layer III. We based our quantitative analysis of patch cross-sectional area and patch density on the CytOx staining found in layer III. The overlain diagram at the bottom indicates the location and thickness of the cortical layers. The asterisk labels layer IVA. Scale bar = 1 mm

distribution led us to base our analyses of patch cross-sectional area and density on layer III staining. Also in agreement with previous studies (Horton, 1984), we observed human patches to be oval when viewed in tangential sections (Figures 5, 6). Adjacent patches appear sometimes to be linked by bridges of CytOx-reactive tissue, giving rise to elongated row-like structures. We observed linkages between adjacent patches to be more frequent at the central vision representation of V1. For example, row-like structures can be observed in several portions of Figure 5, which represents the foveal and parafoveal regions of V1. Despite these bridges, the individuality of patches in a row was still clear (Figures 5, 6) through most of V1.

Three of the six preparations preserved complete a representation of area V1: BH1, BH3, and BH5. The V1 surface area in these hemispheres was 2,415, 1,870, and 2,480 mm^2, respectively (see Figure 3), with average surface area of 2,255 mm^2. The largest V1 surface area in our sample (BH5) was 32% larger than that in the smallest case (BH3).

3.1 | Patch spatial densities

Figure 7a illustrates that, within the binocular representation of human V1, the average patch spatial density decreases significantly with increasing cortical eccentricity (regression coefficient, $p = .004$), from around 1.0 patch/mm^2 in the foveal representation to 0.6 patch/mm^2 at approximately 60° eccentricity. This gentle decrease was attributed primarily to the common occurrence of regions of high patch density (>0.8 patches/mm^2) in parts of V1 expected to represent eccentricities below 5°. At the transition between the binocular and monocular regions, there was a suggestion that this trend reverses to a small degree, with the data suggesting a slightly larger patch density at the monocular crescent (around 0.8 patch/mm^2) near the rostral end of V1, in the depths of the calcarine sulcus. The number of patches per mm^2 at a given eccentricity does not vary consistently with polar angle.

3.2 | Patch cross-sectional area

We found no difference in patch size as a function of eccentricity. Figure 7b shows the average values of patch cross-sectional area across 16 eccentricity bins, which included binocular and monocular visual field

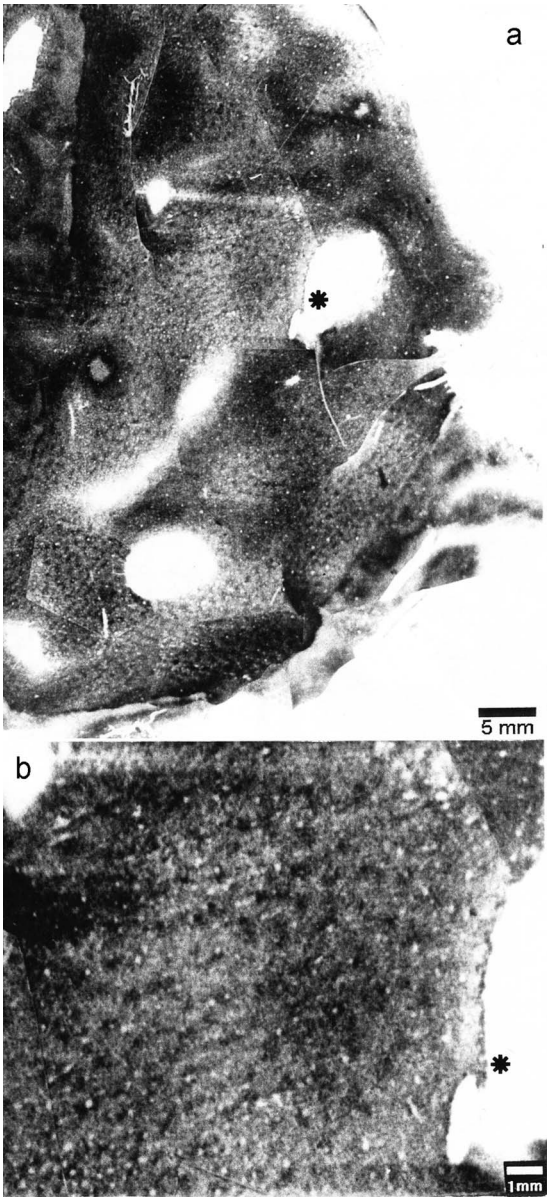

FIGURE 5 Patch morphology in central vision representation of V1. (a) Low magnification photomicrograph of a flattened V1 section stained for CytOx and cut through layer III. Scale bar = 5 mm. The fovea is represented at the bottom left of the figure, while the light-to-dark transition in staining on the upper left corresponds to the V1–V2 border. (b) Higher magnification photomicrograph of the region indicated by the asterisk in pane l (a). Scale bar = 1 mm

J_ID: Customer A_ID: CNE24435 Cadmus Art: CNE24435 Ed. Ref. No.: CASA-JCN-17-0256.R1 Date: 4-April-18 Stage: Page: 6

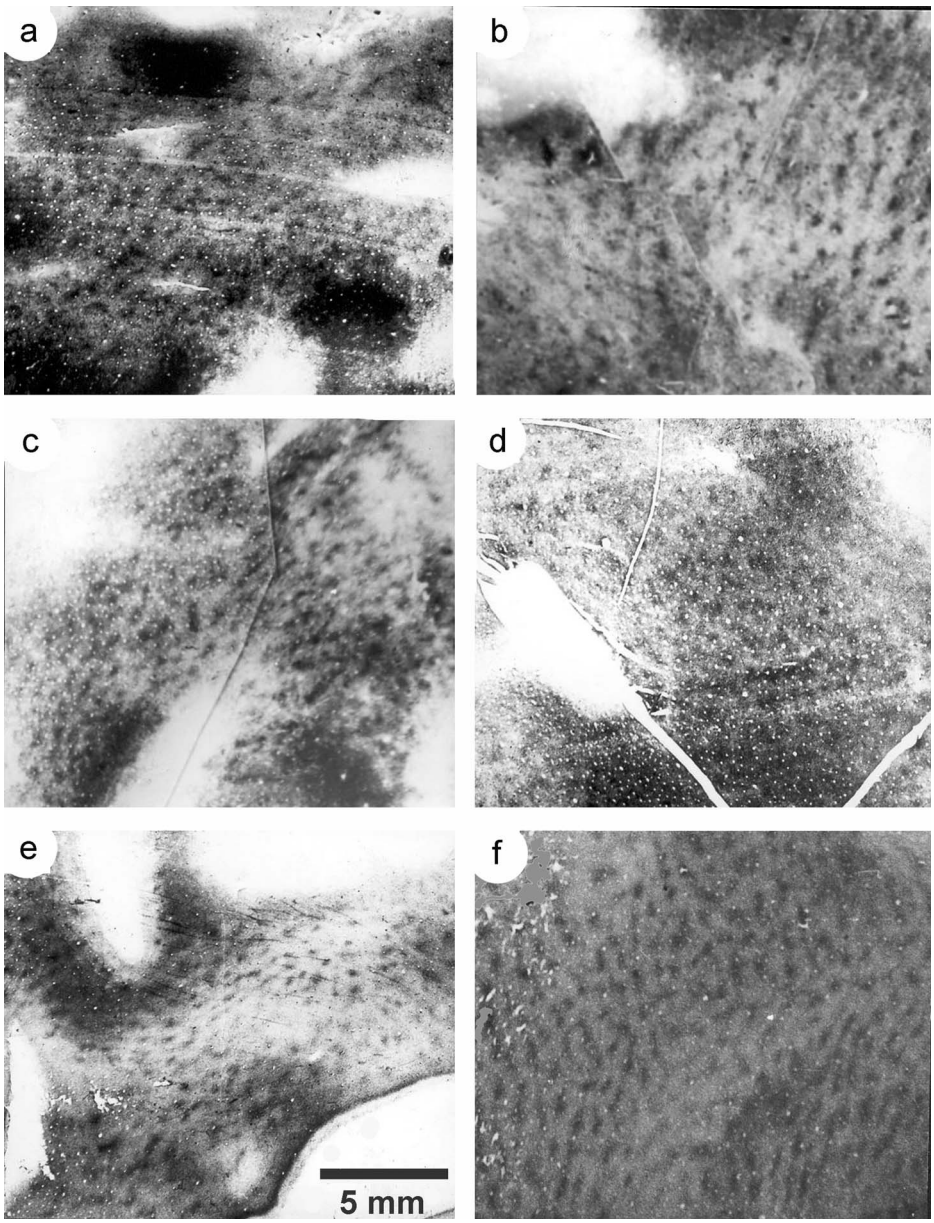

FIGURE 6 Patch morphology across six V1 cases. (a–f) Photomicrograph of flattened V1 sections stained for CytOx and cut through layer III for the corresponding six cases studied (BH1–6). Scale bar = 5 mm. Note that patch morphology can range from round individualized units to multiple elongated structures containing several fused patches

representation. We found no statistical difference across the groups ($p = 0.535$). Despite this homogeneity, we did find a substantial variability in the sizes of individual patches. Across the entire sample, the estimates of patch cross-sectional area varied from approximately 0.2 mm^2 to 0.8 mm^2, with a mean value of 0.32 mm^2, and most occurrences between 0.2 and 0.5 mm^2 (mode = 0.3 mm^2, see Figure 8). There was, in addition, no statistical difference in patch size for the different polar angle representations ($p = .122$). Finally, despite the variations in V1 surface area mentioned above, there were no obvious variations in patch cross-sectional area. In BH3 the mean patch area that was only subtly (<5%) smaller than in BH5 ($p = .003$). Although these estimates are, by nature, approximate (see Methods), we can conclude that systematic changes, if present, are relatively subtle, and below the precision of our procedures.

4 | DISCUSSION

Cytochrome oxidase-rich patches were previously investigated in human V1 by various groups (Horton, 1984, Horton & Hedley-Whyte, 1984; Wong-Riley et al., 1993; Tootell & Taylor, 1995). Here, based on a larger sample, we investigated the characteristics and distribution of patches in human V1. The results show no difference in patch size across the full extent of V1, and also demonstrate that variations in patch density across V1 are quite subtle, particularly when compared to the large variation of functional measures such as the cortical magnification factor (Schira et al., 2007) and population receptive field size (Dumoulin & Wandell, 2008; Harvey & Dumoulin, 2011). These results align well with the hypothesis, derived from studies in non-human

ID: jwweb3b2server Time: 18:07 I Path: //chenas03.cadmus.com/Cenpro/ApplicationFiles/Journals/Wiley/CNE#/Vol00000/180037/Comp/APPFile/JW-CNE#180037

J_ID: Customer A_ID: CNE24435 Cadmus Art: CNE24435 Ed. Ref. No.: CASA-JCN-17-0256.R1 Date: 4-April-18 Stage: Page: 7

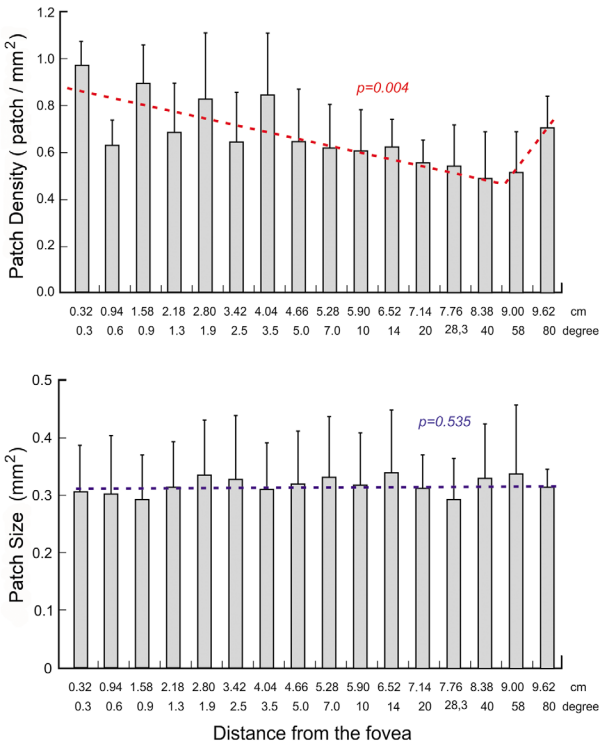

FIGURE 7 Patch density decreases within the V1 binocular region, while patch size remains relatively constant throughout V1 extension. Data from Cases BH1, 3 and 5. (a) Patch density (in blobs/mm^2) as a function of visual eccentricity for the binocular (0.3° to 58°) and monocular (> 60°) representations of the visual field. Note the significant decrease in patch density with increasing eccentricity for the binocular region of V1 ($p = .004$), and the rebound in patch density for the monocular crescent. (b) Patch size (measured in mm^2 as the mean patch cross-sectional area) as a function of visual eccentricity. We found no significant trend in patch size as a function of visual eccentricity ($p = .535$). The abscissa is depicted both in cm (distance from the fovea) and in degrees (visual eccentricity representation) [Color figure can be viewed at wileyonlinelibrary.com]

primates, that V1 is formed by modules of near-constant size, each processing information from a compartment of the visual field. However, it is also clear that the size of the V1 compartment including each patch (or pair of patches, in species where these are associated with ocular dominance columns) is several times smaller than the physiologically measured point-image size (see Chaplin et al., 2013 for a review), suggesting that the visual field represented by neurons within adjacent patches overlaps to a large extent.

4.1 | Correlation between patch size and V1 surface area

We found a substantial variability in V1 surface area across our cases. Previous studies have reported a range of values for the mean surface area of adult human V1 (Brodmann, 1918; Putnam, 1926; Popoff, 1927; Filimonoff, 1932). Part of this variability reflects the distinct methods used for brain histological processing and V1 surface measurement. However, one must acknowledge the fact that our sample is relatively small ($n = 3$ individuals in which we obtained a complete flat mount), and the actual variability in the population is likely to be larger. In one of the largest studies reported, Stensaas, Eddington, and Dobelle (1974) investigated V1 surface area in 52 coronally sectioned human hemispheres using 10% formaldehyde as fixative. In their study, V1 surface area measured for one hemisphere ranged between 1,284 and 3,702 mm^2 (mean = 2,134 mm^2). This average value is only slightly lower than the one we observed in our study using flat-mounted preparations (area = 2,255 mm^2). In another report, Adams et al., (2007) obtained values between 1,986 and 3,477 mm^2 (mean = 2,643 mm^2). Variability of V1 surface area has also been observed in vivo using fMRI (Dougherty et al., 2003; Verghese, Kolbe, Anderson, Egan, & Vidyasagar, 2014). Thus, there is enough experimental evidence to support the notion that the high variability in V1 size is real and substantial (Amunts et al., 2007), and it is likely that this variability translates into individual variations in perceptual performance (Verghese et al., 2014). Condo and Casagrande (1990) proposed a linear relationship between V1 size and the number of CytOx-rich patches across different primate species. Given the large variability in human V1, it would be worth exploring, based on a larger sample, if the same scaling rule applies across individuals of the same species.

4.2 | Quantitative comparisons of patch size and density in humans with other primates

In order to investigate if patch size is systematically correlated with V1 surface area (i.e., V1 size) across different primate species, we compared the size and density of patches in human V1 with those reported for the *Cheirogaleus medius* (Preuss & Kaas, 1996), *Galago senegalensis* (Condo & Casagrande, 1990), *Galago crassicaudatus* (Condo & Casagrande, 1990), *Callitrix jacchus* (Pessoa et al., 1992), *Aotus trivirgatus* (Myerson, Manis, Miezin, & Allman, 1977), *Saimiri sciureus* (Franca, do-Nascimento, Picanço-Diniz, Quaresma, & Silva, 1997; Frahm et al., 1984), *Sapajus apella* (the tufted capuchin monkey, formerly referred to as *Cebus apella*; Rosa et al., 1991; Hess & Edwards, 1987), *Macaca*

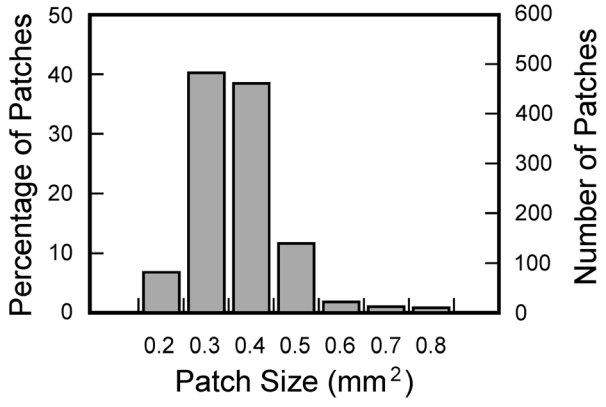

FIGURE 8 Despite the large variability in human V1 patch size, most occurrences cluster in a narrow range. The plot shows the histogram distribution of patch size for the six cases studied, measured both in percentage of occurrences (left *y*-axis) and in number of patches (right *y*-axis)

J_ID: Customer A_ID: CNE24435 Cadmus Art: CNE24435 Ed. Ref. No.: CASA-JCN-17-0256.R1 Date: 4-April-18 Stage: Page: 8

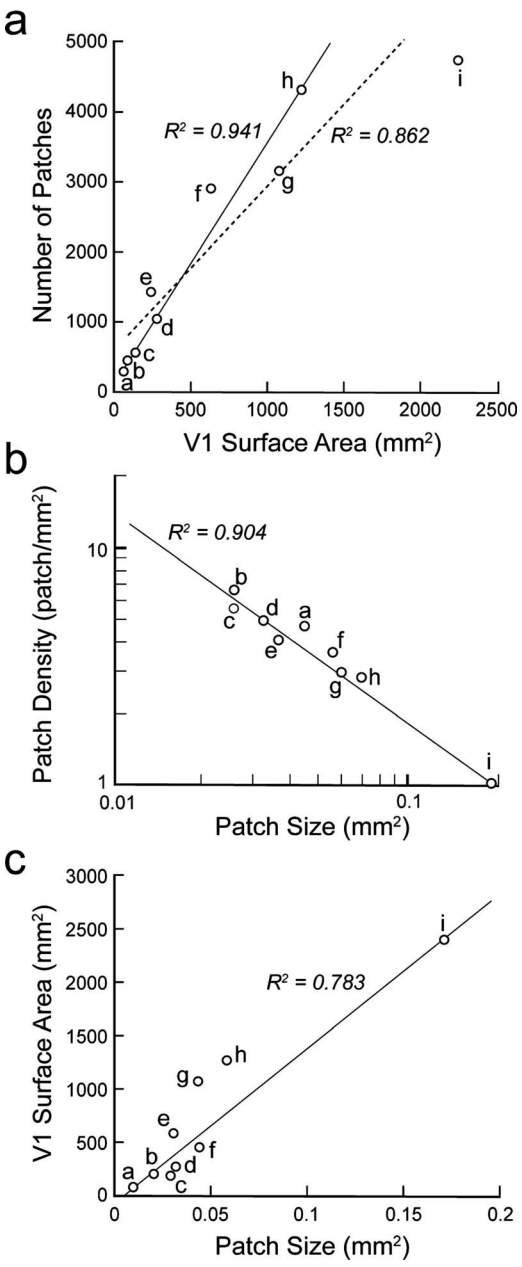

FIGURE 9 Patch size and number are directly related to V1 surface area across different primate species, while patch size is inversely related to patch density. (a) Linear regression between number of V1 patches and V1 surface area across nine primate species (dotted line, $R^2 = 0.862$). The continuous line depicts the linear regression for the data points excluding humans ($R^2 = 0.941$). (b) Linear regression between patch size and patch density plotted on a logarithmic scale for the same nine species studied in (a). Note that the correlation between both variables is inversed and highly linear ($R^2 = 0.993$). (c) Linear correlation between patch size and V1 surface area for the same species studied in (a) and (b). Data points a–i correspond to the following primate species and were obtained from the following sources: *a*, *Cheirogaleus medius* (Preuss & Kaas, 1996); *b*, *Galago senegalensis* (Condo & Casagrande, 1990); *c*, *Galago crassicaudatus* (Condo & Casagrande, 1990); *d*, *Callitrix jacchus* (Pessoa et al., 1992); *e*, *Aotus trivirgatus* (Myerson et al., 1977); *f*, *Saimiri sciureus* (Franca et al., 1997; Frahm, Stephan, and Baron, 1984); *g*, *Sapajus apella* (Rosa et al., 1991; Hess & Edwards, 1987); *h*, *Macaca mulatta* (Farias et al., 1997); *i*, *Homo sapiens* (Marcondes, 1997; Horton & Hedley-Whyte, 1984; and the present study)

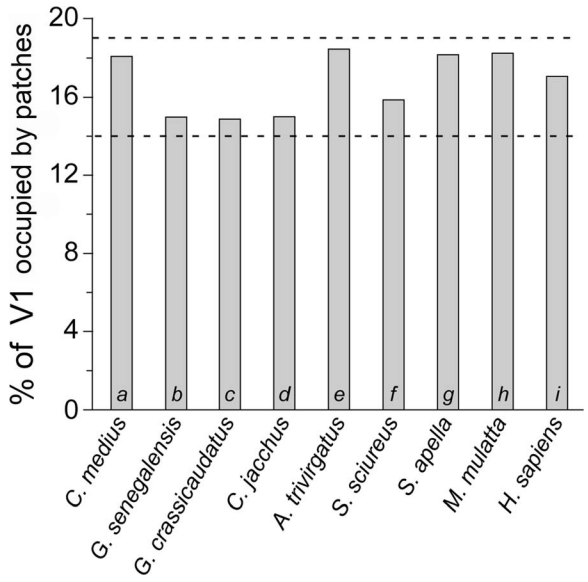

FIGURE 10 The cortical V1 area occupied by patches is fairly constant across species. The plot shows the percentage of V1 surface area occupied by patches across nine different primate species, which includes small and large primates. Labels as depicted in the legend of Figure 9

mulatta (Farias, Gattass, Piñón, & Ungerleider, 1997), and *Homo sapiens* (Marcondes, 1997; Horton & Hedley-Whyte, 1984; and the present study). A similar comparison was first made by Condo and Casagrande (1990), using a smaller range of primate species. They compared CytOx-rich patches both between closely related primate species of different brain sizes and between more distantly related primate species. Their data suggested that the number of V1 patches for species belonging to the same genus is linearly proportional to V1 surface area.

Figure 9a shows the relationship between estimated total patch number and the surface area of primate V1. As proposed by Condo and Casagrande (1990), the correlation between the two measures is striking, suggesting that one should be able to predict the number of V1 patches simply by estimating V1 size: these results show that V1 size and its total number of patches are strongly correlated with one another across different primate species, and that a linear regression can account for at least 86% of the variance between the two variables ($R^2 = 0.862$). If the data point representing human subjects is left out of the analysis, the linear correlation increases ($R^2 = 0.941$), a result which gives some support to Condo and Casagrande (1990), who suggested that humans may be an outlier compared to other primates in what concerns the total number of patches as a function of V1 area. However, this conclusion may require further investigation based on larger samples. In addition, patch density (measured as the number of patches per unit area) decreases with increasing patch size (measured as mean patch cross-sectional area, see Figure 9b). This inverse correlation follows a logarithmic function ($R^2 = 0.904$). Note that humans are placed at one of the extremes within the logarithmic relationship between patch density and patch size, exhibiting the lowest patch density and the largest patch size among the different species being compared (Figure 9c—data point *i*). Macaque (Figure 9c, data point *h*) and capuchin (Figure 9c, data point *g*)

J_ID: Customer A_ID: CNE24435 Cadmus Art: CNE24435 Ed. Ref. No.: CASA-JCN-17-0256.R1 Date: 4-April-18 Stage: Page: 9

monkeys, which have a V1 area ranging from 1,000 to 1,500 mm^2, exhibit medium patch size and medium patch density.

Consistent with a proportional relationship, we found that larger V1 cortices contain larger patches (Figure 9c). Nonetheless, as the size of V1 decreases there is an inferior limit for the decrease of patch size (note the agglomeration of data points *a*–*d*, at the bottom left of Figure 9c). At this point, the relationship between patch density and patch size becomes unclear (Figure 9c). This limit appears to be related to the minimum number of neurons necessary to compose a patch (Gattass et al., 1990b). However, the precise nature of the relationship, particularly among species with small striate cortex, may require further studies in which the histological and data analysis procedures are uniform across species. The different studies we use for comparison here come from different laboratories, and do not sample individuals of similar developmental stage, which may contribute to variance in estimates of patch size, patch density, and V1 area. However, the percentage of V1 area occupied by patches appears to be remarkably similar across the different primate species, with estimates ranging between 14 and 19% (Figure 10).

F10

The two simplest models to explain the above results would be one whereby patch size increases, and patch density decreases, in direct proportion of increasing V1 size, or one where patch size and density remain constant, but the patch number increases linearly with increasing V1 size. The data reviewed above seem to reveal that a more complex combination of factors establishes patch topography during development. Both patch size and patch number increase, but not always in exact proportion to increases in V1 surface area across species (Figure 9a), while keeping the ratio of total patch area/V1 area approximately constant.

In summary, in a same individual, patch size remains approximately constant across visual eccentricities, suggesting that the size of V1 processing modules can be well preserved despite considerable variations in the underlying function organization, such as the cortical magnification factor. Notwithstanding this invariance at the individual level, patch size, number and density can vary across primate species, but with one important constraint: the amount of V1 tissue dedicated to patches remains approximately constant. These findings may impose important constraints on how to interpret patch formation during development, and guide models of formation of columnar systems in primate V1.

Vivien Alice Casagrande made fundamental contributions to two of the key themes that guide this study: the significance of cytochrome oxidase patches in the primate visual cortex (e.g., Lachica & Casagrande, 1992; Casagrande, 1994; Ding & Casagrande, 1997; Boyd & Casagrande, 1999; Boyd, Mavity-Hudson, & Casagrande, 2000) and comparative studies of their characteristics and distribution in different primate brains (Condo & Casagrande, 1990). Her enthusiasm, scientific flair and rigorous application of neuroanatomical techniques have greatly influenced this field of research. In our hearts, she will be sorely missed!

ACKNOWLEDGMENTS

We wish to thank Juliana Soares for her valuable comments on the manuscript. We also wish to thank Edil Saturato da Silva Filho and Liliane Pontes Motta for their skillful technical assistance.

CONFLICT OF INTEREST

We declare no conflict of interest.

AUTHOR CONTRIBUTIONS

All authors had full access to the data and take responsibility for the integrity of the results and the accuracy of the data analysis. MM, RG planned the experiments; MM obtained the materials and relevant consent; MM, MGPR, MF, RG prepared the materials; BL, MF, RG analyzed the data; all authors reviewed the data, and cooperatively prepared the manuscript.

ORCID

Bruss Lima http://orcid.org/0000-0001-6865-2900
Ricardo Gattass http://orcid.org/0000-0002-0321-1490

REFERENCES

Adams, D. L., Sincich, L. C., & Horton, J. C. (2007). Complete pattern of ocular dominance columns in human primary visual cortex. *Journal of Neuroscience*, *27*, 10391–10403.

Amunts, K., Armstrong, E., Malikovic, A., Homke, L., Mohlberg, H., Schleicher, A., & Zilles, K. (2007). Gender-specific left-right asymmetries in human visual cortex. *Journal of Neuroscience*, *27*, 1356–1364.

Bartfeld, E., & Grinvald, A. (1992). Relationships between orientation-preference pinwheels, cytochrome oxidase blobs, and ocular-dominance columns in primate striate cortex. *Proceedings of the National Academy of Sciences United States of America*, *89*, 11905–11909.

Blasdel, G. G., & Salama, G. (1986). Voltage-sensitive dyes reveal a modular organization in monkey striate cortex. *Nature*, *321*, 579–585.

Boyd, J. D., & Casagrande, V. A. (1999). Relationships between cytochrome oxidase (CO) blobs in primate primary visual cortex (V1) and the distribution of neurons projecting to the middle temporal area (MT). *The Journal of Comparative Neurology*, *409*, 573–591.

Boyd, J. D., Mavity-Hudson, J. A., & Casagrande, V. A. (2000). The connections of layer 4 subdivisions in the primary visual cortex (V1) of the owl monkey. *Cerebral Cortex*, *10*, 644–662.

Brodmann, K. (1918). Individuelle Variationen der Sehsphäre und ihr Bedeutung für die Klinik der Hinterhauptschusse. *Allgz Psychiat (Berlin)*, *74*, 564–568.

Carroll, E. W., & Wong-Riley, M. T. T. (1984). Quantitative light- and electron microscopic analysis of cytochrome oxidase-rich zones in the striate cortex of the squirrel monkey. *Journal Comparative Neurology*, *222*, 1–17.

Casagrande, V. A. (1994). A third parallel visual pathway to primate area V1. *Trends in Neurosciences*, *17*, 305–310.

Chaplin, T. A., Yu, H. H., & Rosa, M. G. (2013). Representation of the visual field in the primary visual area of the marmoset monkey: Magnification factors, point-image size, and proportionality to retinal ganglion cell density. *Journal of Comparative Neurology*, *521*, 1001–1019.

Condo, G. J., & Casagrande, V. A. (1990). Organization of cytochrome oxidase staining in the visual cortex of nocturnal primates (Galago crassicaudatus and Galago senegalensis): I. Adult patterns. *Journal Comparative Neurology*, *293*, 632–645.

Cusick, C. G., Gould, H. J., 3rd, & Kaas, J. H. (1984). Interhemispheric connections of visual cortex of owl monkeys (*Aotus trivirgatus*), marmosets (*Callithrix jacchus*), and galagos (*Galago crassicaudatus*). *Journal Comparative Neurology*, *230*, 311–336.

Ding, Y., & Casagrande, V. A. (1997). The distribution and morphology of LGN K pathway axons within the layers and CO blobs of owl monkey V1. *Visual Neuroscience*, *14*, 691–704.

Dougherty, R. F., Koch, V. M., Brewer, A. A., Fischer, B., Modersitzki, J., & Wandell, B. A. (2003). Visual field representations and locations of visual areas V1/2/3 in human visual cortex. *Journal of Vision*, *3*, 586–598.

Dumoulin, S. O., & Wandell, B. A. (2008). Population receptive field estimates in human visual cortex. *Neuroimage*, *39*, 647–660.

Farias, M. F., Gattass, R., Piñón, M. C., & Ungerleider, L. G. (1997). Tangential distribution of cytochrome oxidase-rich blobs in the primary visual cortex of macaque monkeys. *Journal Comparative Neurology*, *386*, 217–228.

Filimonoff, I. (1932). Über die Variabilität der Grosshirnrindenstruktur, II. Regio occipitalis beim erwachsenen Menschen. *Journal Psychological Neurology*, *44*, 1–96.

Florence, S. L., & Kaas, J. H. (1992). Ocular dominance columns in area 17 of Old World macaque and talapoin monkeys: Complete reconstructions and quantitative analyses. *Visual Neuroscience*, *8*, 449–462.

Frahm, H. D., Stephan, H., & Baron, G. (1984). Comparison of brain structure volumes in insectivora and primates. V. Area striata (AS). *Journal für Hirnforschung*, *25*, 537–557.

Franca, J. G., do-Nascimento, J. L., Picanço-Diniz, C. W., Quaresma, J. A., Silva, A. L. (1997). NADPH-diaphorase activity in area 17 of the squirrel monkey visual cortex: neuropil pattern, cell morphology and laminar distribution.. *Braz J Med Biol Res.*, *30*, 1093–1105.

Gattass, R., Sousa, A. P. B., & Rosa, M. G. P. (1987). Visual topography of V1 in the *Cebus* monkey. *Journal Comparative Neurology*, *259*, 529–548.

Harvey, B. M., & Dumoulin, S. O. (2011). The relationship between cortical magnification factor and population receptive field size in human visual cortex: Constancies in cortical architecture. *Journal of Neuroscience*, *31*, 13604–13612. https://doi.org/10.1523/JNEUROSCI.2572-11.2011

Hendrickson, A. E. (1985). Dots, stripes and columns in monkey visual cortex. *Trends in Neuroscience*, *8*, 406–410.

Hess, D. T., & Edwards, M. A. (1987). Anatomical demonstration of ocular segregation in the retinogeniculocortical pathway of the New World capuchin monkey *(Cebus apella)*. *Journal Comparative Neurology*, *264*, 409–420.

Horton, J. C. (1984). Cytochrome oxidase patches: A new cytoarchitectonic feature of monkey visual cortex. *Philosophical Transactions of the Royal Society (London) B Biological Sciences*, *304*, 199–253.

Horton, J. C., & Hedley-Whyte, E. T. (1984). Mapping of cytochrome oxidase patches and ocular dominance columns in human visual cortex. *Philosophical Transactions of the Royal Society (London) B Biological Sciences*, *304*, 255–272.

Horton, J. C., & Hocking, D. R. (1996). Pattern of ocular dominance columns in human striate cortex in strabismic amblyopia. *Visual Neuroscience*, *13*, 787–795.

Horton, J. C., & Hoyt, W. F. (1991). The representation of the visual field in human striate cortex: A revision of the classic Holmes map. *Archives of Ophthalmology*, *109*, 816–824.

Horton, J. C., & Hubel, D. G. (1981). Regular patchy distribution of cytochrome oxidase staining in primary visual cortex of macaque monkey. *Nature*, *292*, 762–764.

Hubel, D. H., & Wiesel, T. N. (1977). Functional architecture of macaque monkey visual cortex: Ferrier lecture. *Proceedings of the Royal Society of London B, Biological Sciences*, *198*, 1–59.

Lachica, E. A., & Casagrande, V. A. (1992). Direct W-like geniculate projections to the cytochrome oxidase (CO) blobs in primate visual cortex: Axon morphology. *Journal Comparative Neurology*, *319*, 141–158.

Livingstone, M. S., & Hubel, D. H. (1984). Anatomy and physiology of a color system in the primate visual cortex. *Journal of Neuroscience*, *4*, 309–356.

Lorente de Nó, R. (1949). In J. F. Fulton (Ed.), *Physiology of the nervous system* (pp. 288–312). London: Oxford University Press.

Löwel, S., & Singer, W. (1987). The pattern of ocular dominance columns in flat-mounts of the cat visual cortex. *Experimental Brain Research*, *68*, 661–666.

Marcondes, M. (1997). Tangential distribution and plasticity of cytochrome oxidase blobs of V1 in normal adult humans and in humans with chronic retinal lesions. PhD thesis, IBCCF/UFRJ, Federal University of Rio de Janeiro.

Myerson, J., Manis, P. B., Miezin, F. M., & Allman, J. M. (1977). Magnification in striate cortex and retinal ganglion cell layer of owl monkey: A quantitative comparison. *Science*, *198*, 855–857.

Mountcastle, V. B. (1978). In G.M. Edelman & V.B. Mountcastle (Eds.), *The mindful brain: Cortical organization and the group-selective theory of higher brain function* (pp. 7–50). Boston: MIT Press.

Olavarria, J., & Van Sluyters, R. C. (1985). Unfolding and flattening the cortex of gyrencephalic brains. *Journal of Neuroscience Methods*, *15*, 191–202.

Pessoa, V. F., Abrahão, J. C., Pacheco, R. A., Pereira, L. C., Magalhães-Castro, B., & Saraiva, P. E. (1992). Relative sizes of cortical visual areas in marmosets: Functional and phylogenetic implications. *Experimental Brain Research*, *88*, 459–462.

Popoff, N. (1927). Zur Kenntnis der Grösse der Area striate und die Methodik ihrer Ausmessung. *Journal of Psychological Neurology*, *34*, 238–242.

Preuss, T. M., & Kaas, J. H. (1996). Cytochrome oxidase 'blobs' and other characteristics of primary visual cortex in a lemuroid primate, *Cheirogaleus medius*. *Brain Behavior and Evolution*, *47*, 103–112.

Purves, D., & LaMantia, A. (1993). Development of blobs in the visual cortex of macaques. *Journal Comparative Neurology*, *334*, 169–175.

Putnam, T. (1926). Studies on the central visual connections. III. The general relationships between the external geniculate body, optic radiations and visual cortex in man. Report of two cases. *Archives of Neurology and Psychiatry of London*, *16*, 683–707.

Rosa, M. G. P., Gattass, R., & Fiorani, M. Jr. (1988). Complete pattern of ocular dominance stripes in V1 of a New World monkey, *Cebus apella*. *Experimental Brain Research*, *72*, 645–648.

Rosa, M. G. P., Gattass, R., & Soares, J. G. M. (1991). A quantitative analysis of cytochrome oxidase-rich patches in the primary visual cortex of *Cebus* monkeys: Topographic distribution and effects of late monocular enucleation. *Experimental Brain Research*, *84*, 195–209.

Rosa, M. G. P., Gattass, R., Fiorani, M. Jr., & Soares, J. G. M. (1992). Laminar, columnar and topographic aspects of ocular dominance in the primary visual cortex of Cebus monkeys. *Experimental Brain Research*, *88*, 249–264.

Schira, M. M., Tyler, C. W., & Rosa, M. G. P. (2012). Brain mapping: The (un)folding of striate cortex. *Current Biology*, *22*, R1051–R1053.

Schira, M. M., Wade, A. R., Tyler, C. W. (2007). Two-dimensional mapping of the central and parafoveal visual field to human visual cortex. *J Neurophysiol.*, *97*, 4284–6584295.

Sereno, M. I., Dale, A. M., Reppas, J. B., Kwong, K. K., Belliveau, J. W., Brady, T. J., . . . Tootell, R. B. (1995). Borders of multiple visual areas in humans revealed by functional magnetic resonance imaging. *Science*, *268*, 889–893.

Silverman, M. S., & Tootell, R. B. H. (1987). Modified technique for cytochrome oxidase histochemistry: Increased staining intensity and compatibility with the 2-deoxyglucose autoradiography. *Journal of Neuroscience Methods*, *19*, 1–10.

Sincich, L. C., Adams, D. L., & Horton, J. C. (2003). Complete flatmounting of the macaque cerebral cortex. *Visual Neuroscience*, *20*, 663–686.

Solodkin, A., & Van Hoesen, G. W. (1996). Entorhinal cortex modules of the human brain. *Journal Comparative Neurology*, *365*, 610–617.

Solomon, S. G. (2002). Striate cortex in dichromatic and trichromatic marmosets: Neurochemical compartmentalization and geniculate input. *Journal Comparative Neurology*, *450*, 366–381.

Stensaas, S. S., Eddington, D. K., & Dobelle, W. H. (1974). The topography and variability of the primary visual cortex in man. *Journal of Neurosurgery*, *40*, 747–755.

Tigges, M., Hendrickson, A. E., & Tigges, J. (1984). Anatomical consequences of long-term monocular eyelid closure on lateral geniculate nucleus and striate cortex in squirrel monkey. *Journal Comparative Neurology*, *227*, 1–13.

Tootell, R. B., & Taylor, J. B. (1995). Anatomical evidence for MT and additional cortical visual areas in humans. *Cerebral Cortex*, *5*, 39–55.

Tootell, R. B., Silverman, M. S., De Valois, R. L., & Jacobs, G. H. (1983). Functional organization of the second cortical visual area in primates. *Science*, *220*, 737–739.

Tootell, R. B. H., & Silverman, M. S. (1985). Two methods for flat-mounting cortical tissue. *Journal of Neuroscience Methods*, *15*, 177–190.

Tootell, R. B. H., Hamilton, S. L., & Silverman, M. S. (1985). Topography of cytochrome oxidase activity in owl monkey cortex. *Journal of Neuroscience*, *5*, 2786–2800.

Trusk, T. C., Kaboord, W. S., & Wong-Riley, M. T. T. (1990). Effects of monocular enucleation, tetrodotoxin, and lid suture on cytochrome oxidase reactivity in supragranular puffs of adult macaque striate cortex. *Visual Neuroscience*, *4*, 185–204.

Ts'o, D. Y., Frostig, R. D., Lieke, E. E., & Grinvald, A. (1990). Functional organization of primate visual cortex revealed by high resolution optical imaging. *Science*, *249*, 417–420.

Valverde Salzmann, M. F., Bartels, A., Logothetis, N. K., & Schüz, A. (2012). Color blobs in cortical areas V1 and V2 of the new world monkey *Callithrix jacchus*, revealed by non-differential optical imaging. *Journal of Neuroscience*, *32*, 7881–7894.

Verghese, A., Kolbe, S. C., Anderson, A. J., Egan, G. F., & Vidyasagar, T. R. (2014). Functional size of human visual area V1: A neural correlate of top-down attention. *Neuroimage*, *93*, 47–52. https://doi.org/10.1016/j.neuroimage.2014.02.023. Epub 2014 Feb 28.

Wong-Riley, M., & Carroll, E. W. (1984). Effect of impulse blockage on cytochrome oxidase activity in monkey visual system. *Nature*, *307*, 262–264.

Wong-Riley, M. T., Hevner, R. F., Cutlan, R., Earnes, M., Egan, R., Frost, J., & Nguyen, T. (1993). Cytochrome oxidase in the human visual cortex: Distribution in the developing and the adult brain. *Visual Neuroscience*, *10*, 41–58.

How to cite this article: Marcondes M, Rosa MGP, Fiorani M, Lima B, Gattass R. Distribution of cytochrome oxidase-rich patches in human primary visual cortex. *J Comp Neurol.* 2018;00:1–11. https://doi.org/10.1002/cne.24435

SGML and CITI Use Only
DO NOT PRINT

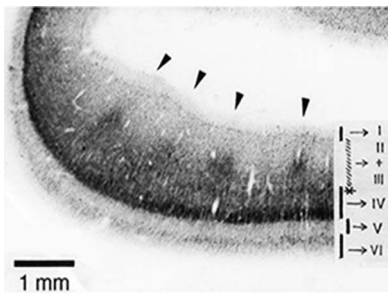

Human patch profile across V1 cortical layers. Photomicrograph of a coronal section through the calcarine fissure stained for CytOx. Patches (shown by arrow heads) are most evident in layers II and III of V1, especially in the middle of layer III. The overlain diagram at the bottom indicates the location and thickness of the cortical layers. The asterisk labels layer IVa.